NeuroImage: Clinical 13 (2017) 130–137

Contents lists available at ScienceDirect

NeuroImage: Clinical

journal homepage: www.elsevier.com/locate/ynicl

Regional correlations between [^{11}C]PIB PET and post-mortem burden of amyloid-beta pathology in a diverse neuropathological cohort

Sang Won Seo[a,b,c,d,*,1], Nagehan Ayakta[a,b,c,1], Lea T. Grinberg[a,e], Sylvia Villeneuve[b,f], Manja Lehmann[a,g], Bruce Reed[h,i], Charles DeCarli[i], Bruce L. Miller[a], Howard J. Rosen[a], Adam L. Boxer[a], James P. O'Neil[c], Lee-Way Jin[j], William W. Seeley[a], William J. Jagust[a,b,c], Gil D. Rabinovici[a,b,c]

[a] Memory and Aging Center, Department of Neurology, University of California, San Francisco, USA
[b] Helen Wills Neuroscience Institute, University of California, Berkeley, USA
[c] Lawrence Berkeley National Laboratory, USA
[d] Departments of Neurology, Samsung Medical Center, Sungkyunkwan University School of Medicine, Republic of Korea
[e] Department of Pathology, University of California, San Francisco, USA
[f] Department of Psychiatry, McGill University, Montreal, Canada
[g] Dementia Research Centre, University College London, London, United Kingdom
[h] Center for Scientific Review, National Institutes of Health, Bethesda, MD, USA
[i] Department of Neurology, School of Medicine, University of California, Davis, USA
[j] Department of Pathology and Laboratory Medicine, University of California, Davis, USA

ARTICLE INFO

Article history:
Received 24 May 2016
Received in revised form 6 November 2016
Accepted 9 November 2016
Available online 11 November 2016

Keywords:
Imaging
Pathology
Amyloid
Alzheimer's disease

ABSTRACT

Imaging-pathological correlation studies show that *in vivo* amyloid-β (Aβ) positron emission tomography (PET) strongly predicts the presence of significant Aβ pathology at autopsy. We sought to determine whether regional PiB-PET uptake would improve sensitivity for amyloid detection in comparison with global measures (experiment 1), and to estimate the relative contributions of different Aβ aggregates to *in vivo* PET signal (experiment 2). In experiment 1, 54 subjects with [^{11}C] PiB-PET during life and postmortem neuropathologic examination (85.2% with dementia, interval from PET to autopsy 3.1 ± 1.9 years) were included. We assessed Thal amyloid phase (N = 36) and CERAD score (N = 54) versus both global and regional PiB SUVRs. In experiment 2 (N = 42), PiB SUVR and post-mortem amyloid β burden was analyzed in five customized regions of interest matching regions sampled at autopsy. We assessed the relative contribution of neuritic plaques (NPs), diffuse plaques (DPs) and cerebral amyloid angiopathy (CAA) to regional PIB SUVR using multi-linear regression. In experiment 1, there were no differences in Area Under the Curve for amyloid phase ≥ A2 and CERAD score ≥ C2 between global and highest regional PiB SUVR ($p = 0.186$ and 0.230). In experiment 2, when NPs, DPs, and/or CAA were included in the same model, moderate to severe NPs were independently correlated with PiB SUVR in all regions except for the inferior temporal and calcarine ROI (β = 0.414–0.804, $p < 0.05$), whereas DPs were independently correlated with PiB SUVR in the angular gyrus ROI (β = 0.446, $p = 0.010$). CAA was also associated with PiB SUVR in the inferior temporal and calcarine ROI (β = 0.222–0.355, $p < 0.05$). In conclusion, global PiB-PET SUVR performed as well as regional values for amyloid detection in our cohort. The substrate-specific binding of PiB might differ among the brain specific regions.

1. Introduction

Imaging-pathological correlation studies show that *in vivo* amyloid-β (Aβ) positron emission tomography (PET) strongly predicts the presence of significant Aβ pathology at autopsy (Clark et al., 2012; Curtis et al., 2015; Ikonomovic et al., 2008; Sabri et al., 2015). The majority of these studies have dichotomized Aβ-PET results based on either a visual read or a global measure of cortical tracer retention, and compared this classification to the maximal density of neuritic plaques (NPs). However, Aβ-PET ligands such as carbon-11 labelled Pittsburgh Compound-B ([^{11}C] PiB) have been shown to also bind *in vitro* to diffuse plaques (DPs) and cerebral amyloid angiopathy (CAA) (Lockhart et al., 2007). Understanding the relative contributions of different Aβ aggregate types to *in vivo* signal is critical, particularly since NPs are more strongly associated with cognitive decline than DPs and CAA (Dickson et al., 1988). Furthermore, while Aβ is usually widely distributed in the association neocortex by the onset of cognitive symptoms (Ogomori et al.,

* Corresponding author at: UCSF Memory & Aging Center, 675 Nelson Rising Lane, Suite 190, San Francisco, CA 94143-1207, USA.
E-mail address: sangwonseo@empal.com (S.W. Seo).
[1] These authors contributed equally to this work.

http://dx.doi.org/10.1016/j.nicl.2016.11.008

1989), recent studies have proposed that specific cortical hub regions may show the earliest Aβ deposition and thus may be more sensitive in patients at early stages of Aβ accumulation (Mintun et al., 2006; Mormino et al., 2012; Villeneuve et al., 2015). With the move in the field towards early detection of less severe Aβ burdens and early intervention, it is important to determine whether earlier detection of Aβ pathology may be possible by using regional rather than global PET thresholds.

In this study, we investigated these questions in a cohort of patients who underwent PiB-PET during life and post-mortem brain autopsy. We hypothesized that regional PiB retention would be more sensitive to Aβ pathology than global PiB retention. We further hypothesized that PiB binding would correlate more strongly with NPs than other Aβ aggregates, given their higher fibrillar content (compared to DPs) and greater overall mass in most patients (compared to CAA).

2. Subjects and methods

2.1. Participants

Participants were enrolled in longitudinal studies of aging and dementia at the University of California, San Francisco Memory and Aging Center (UCSF-MAC, N = 56) or the University of California, Davis (UCD, N = 11) (Fig. 1). Fifty of the 67 were included in a previous study relating the Consortium to Establish a Registry for Alzheimer's disease (CERAD) score and global [^{11}C]PiB-PET retention (Villeneuve et al., 2015). Clinical diagnosis was established at a multi-disciplinary conference applying standard research criteria for mild cognitive impairment (MCI) and dementia syndromes (Albert et al., 2011; Armstrong et al., 2013; Gorno-Tempini et al., 2011; McKhann et al., 2011; Petersen, 2004; Rascovsky et al., 2011). Our recruitment was enriched for patients with clinical Alzheimer's disease (AD) or frontotemporal dementia (FTD), and only a small minority had MCI or normal cognition at the time of PET (Table 1). We obtained written consent from each patient or their surrogate decision makers, and the study was approved by the Institutional Review Boards of UCSF, UCD and Lawrence Berkeley National Laboratory.

2.2. MR imaging

MR images were obtained on two 1.5 T instruments (Siemens Magnetom Avanto and Vision), a 3T instrument (Siemens Tim Trio) and a 4T instrument (Bruker/MedSpec). Acquisition parameters have been described previously (Mormino et al., 2012). For this study T1 images were used only for definition of the cerebellar gray matter reference region in native space (using FreeSurfer v 5.1 software), and for tissue segmentation and spatial warping to the Montreal Neurological Institute template (using statistical parametric mapping, SPM8; http://www.fil.ion.ucl.ac.uk/spm).

2.3. PET acquisition and pre-processing

All subjects underwent PET imaging with [^{11}C] PiB at Lawrence Berkeley National Laboratory on a Siemens ECAT EXACT HR camera (N = 66) or a Siemens Biograph PET/CT scanner (N = 1) as described in a previous study (Villeneuve et al., 2015). Approximately 15 mCi of [^{11}C] PiB was injected intravenously. The imaging protocol varied depending on study, but all subjects had images collected at t = 50–70 min post-injection except for one, who had data acquired between t = 55–70 min. PET frames were realigned, co-registered to the subject's MP-RAGE MRI sequence, then normalized to mean activity in the cerebellar gray matter in order to generate Standardized Uptake Value Ratios (SUVR) images (Villeneuve et al., 2015).

2.4. Neuropathological examination

Brain autopsies were performed by the UCSF Neurodegenerative Disease Brain Bank (UCSF-NDBB, N = 49), UCSF-Department of Pathology (N = s4), UCD (11), University of Pennsylvania (1), University of California Los Angeles (1) and Mayo Clinic Jacksonville (1). Pathological

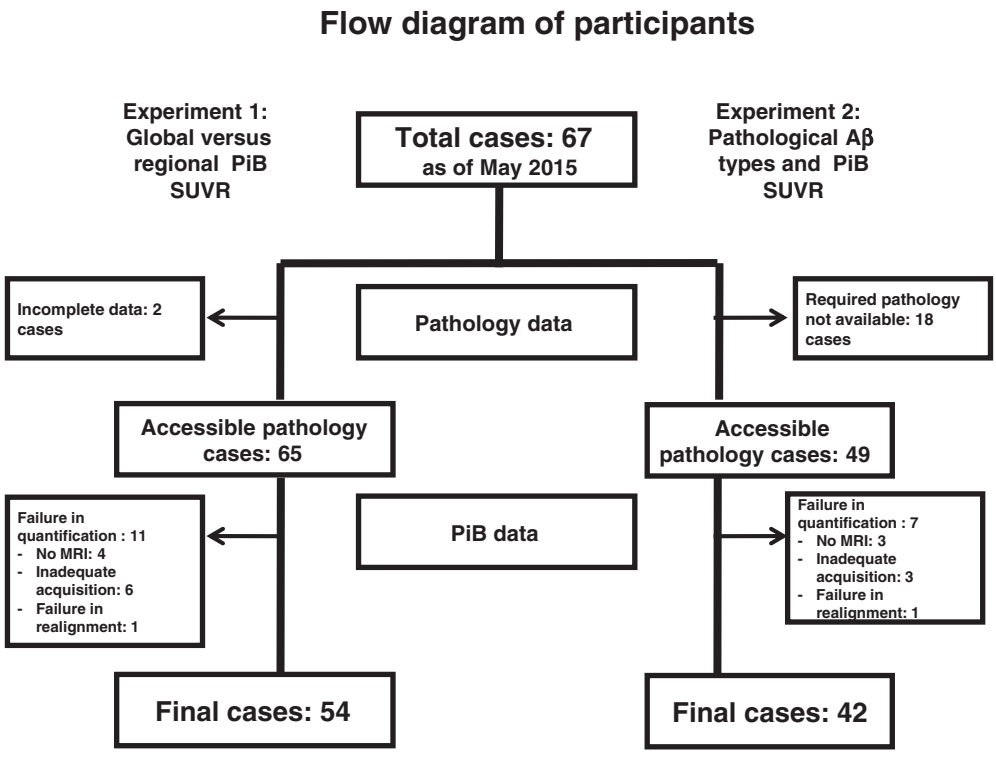

Fig. 1. Flow chart of study participants. Aβ = Amyloid β; PiB = Pittsburgh Compound-B; SUVR = standardized uptake value ratio.

Table 1
Participant characteristics.

Characteristics		Experiment 1: global versus regional PiB SUVR (N = 54)	Experiment 2: pathological Aβ types and PiB SUVR (N = 42)
Age at PET		68.1 (8.8), range 51.0–89.0	66.1 (7.9), range 51.0–89.0
Education		15.6 (2.8), range 12.0–22.0	15.7 (2.8), range 12.0–20.0
Sex (M/F)		33/21	24/18
Time from PET to death (years)		3.1 (1.9), range 0.2–8.3	3.3 (1.9), range 0.2–8.3
MMSE		21.0 (7.3), range 0–29	20.9 (7.2), range 0–29
CDR sum of boxes		6.5 (4.4), range 0–18	6.4 (4.5), range 0–18
APOE4 genotype (carrier/non-carrier)		15/36	14/26
Clinical diagnosis at PET		FTD[a](33), AD (12), VaD (1), MCI (6), NC (2)	FTD[a] (29), AD (11), MCI (2)
Primary neuropathological diagnosis		FTLD[b] (31), AD (18), VaD (4), AGD (1)	FTLD[b] (30), AD (12)
Density (absent, sparse, moderate, frequent) of NPs/DPs/involvement in CAA[c] in			
Cingulate	Anterior		(22,0,7,13)/(20,6,2,14)/(32,4,4,2)
Frontal	Middle		(20,1,5,15)/(16,4,7,14)/(29,5,5,2)
Temporal	Inferior		(21,2,4,15)/(17,2,5,18)/(29,3,7,3)
	Angular		(21,1,1,18)/(15,9,6,11)/(30,3,5,3)
	Calcarine		(20,5,3,13)/(13,6,9,13)/(27,5,4,5)
Thal amyloid phase (A0/A1/A2/A3) (N = 36)		9/13/3/11	
CERAD scores for NP (C0/C1/C2/C3) (N = 54)		22/6/3/23	
ADNC levels (not/low/intermediate/high) (N = 46)		9/22/5/10	

Aβ = Amyloid β; PiB = Pittsburgh Compound-B; SUVR = standardized uptake value ratio; N = number; PET = positron emission tomography; MMSE = Mini-mental state examination; CDR = clinical dementia rating; *APOE* = apolipoprotein E; FTD = frontotemporal dementia; AD = Alzheimer's disease; MCI = mild cognitive impairment; FTLD = frontotemporal lobar degeneration; VaD = vascular dementia; AGD = argyrophilic grain disease; NPs = neuritic plaques; DPs = diffuse plaques; CAA = cerebral amyloid angiopathy; CERAD = Consortium to Establish a Registry for Alzheimer's Disease; ADNC = Alzheimer's disease neuropathological changes.

[a] Clinical syndromes included: corticobasal syndrome (CBS; 7), behavioral-variant FTD (5), FTD and amyotrophic lateral sclerosis (3), non-fluent variant primary progressive aphasia (nfvPPA; 8), nfvPPA/CBS (1), semantic variant PPA (5).

[b] FTLD neuropathological subtypes: FTLD-TDP (12), corticobasal degeneration (8), Pick's disease (7), progressive supranuclear palsy (1), FTLD with non-specific 4 repeat tauopathy (1).

[c] No involvement, involvement in leptomeningeal vessels, involvement in cortical vessels and involvement in subcortical vessels.

assessments were performed using institution-specific protocols (Villeneuve et al., 2015). All autopsies included tissue sampling in regions relevant to the differential diagnosis of dementia based on published consensus criteria (Hyman et al., 2012; Mackenzie et al., 2010). Blocks were embedded in paraffin wax, cut into 8 micron-thick sections, and stained with hematoxylin/eosin. Immunohistochemistry for Aβ (4G8, 1:2000, Covance, NJ) was performed in all cases. Immunohistochemistry for hyperphosphorylated tau (CP-13, 1:500, gift from Peter Davies, NY), α-synuclein (1:500, LB509, Invitrogen, CA), and transactive response DNA binding protein 43 (TDP-43, 1:500, Proteintech, Chicago, IL). For all UCSF autopsies, immunoperoxidase staining was performed using an avidin-biotin complex detection system (Vectastain ABC kit; Vector Laboratories, Burlingame, CA) with 3,3 diaminobenzidine as the chromogen. Slides were pretreated for antigen retrieval by immersion in citrate pH 6.0 in an autoclave at 121 °C for 5 min. Primary antibodies were incubated overnight at 4 °C and species-specific biotinylated secondary antibodies were incubated for one hour at room temperature. Other institutions' protocols were similar. Neuritic and diffuse plaques were counted in sections immunostained for Aβ. Neuritic plaques were defined as plaques with a distinctive core or a plaque with well-defined borders and neuritic components. Diffuse plaques lacked a morphologically identifiable substructure. In both cases, neuritic and diffuse plaques' densities were based on the highest density of each type of plaques found in each area. Sections were rated unadjusted for age and rated in the following manner: 1–5 plaques in a 100× field were classified as sparse, 6–14 as moderate and ≥15 as frequent.(Montine et al., 2012)

2.5. Experiment 1: global versus regional PiB SUVR

In order to determine whether global or regional PiB SUVR would better predict pathological Aβ burden or Alzheimer's Disease Neuropathological Change (ADNC) (Hyman et al., 2012), autopsy reports were reviewed by an experienced neurologist (S.W.S) who extracted Thal phases for amyloid plaques (no plaques = 0, Phase1–2 = A1, Phase3 = A2, Phase4–5 = A3), Braak stages for neurofibrillary degeneration (no forebrain NFTs = 0, Stage1–2 = B1, Stage3–4 = B2, Stage5–6 = B3), the Consortium to Establish a Registry for Alzheimer's disease (CERAD) scores for neuritic plaques (no neuritic plaques = 0, sparse = C1, moderate = C2, frequent = C3), and ADNC scores according to recently revised NIA-AA guidelines (Hyman et al., 2012). Thal amyloid phase of "A2 to A3", CERAD scores of "C2 to C3", and ADNC levels of "intermediate to high" were considered to be positive. We obtained Thal phases in only 36 cases because Aβ burden was not assessed in the subcortical structures, midbrain and cerebellum before 2012. ADNC levels, however, could be assessed in 46 cases because in some cases ADNC may be determined in spite of missing data elements. For instance, if cases had sparse NPs and Braak stage 2, then their ADNC levels would be rated as low regardless of Thal phase.

To estimate mean cortical PiB retention, we created a "PiB index" region of interest (ROI) as described in a previous study (Rabinovici et al., 2010). The PiB index ROI included the following regions defined within the Automated Anatomical Labeling (AAL) atlas (Tzourio-Mazoyer et al., 2002): superior frontal gyrus, middle frontal gyrus, frontal superior/middle/inferior orbital gyri, superior medial frontal gyrus, inferior operculum, inferior triangularis, rolandic operculum, supplementary motor areas, rectus, olfactory bulb, insula, anterior cingulate, superior/middle/inferior temporal, superior/inferior parietal lobule, supramarginal gyrus, angular gyrus, posterior cingulate, precuneus, and middle cingulate. These regions consistently show high PIB retention in studies of AD and aging (Mormino et al., 2012; Rabinovici et al., 2010). Regional PiB SUVR values were also extracted from individual ROIs defined in the AAL atlas.

The global PiB index was extracted in template space across voxels with a gray-matter probability of at least 30% within the PiB index region of interest. In 3 subjects, regions of cortical stroke were masked and not included in the target regions of interest (ROI) for calculation of PiB index. A total of 11 cases were not included in this study because of difficulty with PiB data quantification: missing MRI data needed to generate quantitative values for PIB retention (N = 4), inadequate PiB acquisition (N = 6), and failure of realignment due to subject motion (N = 1). Thus, the final sample for analysis included 54 individuals with both quantitative PiB-PET data and Aβ assessment at autopsy (Fig. 1).

2.6. Experiment 2: pathological Aβ types and PiB SUVR

To investigate the correlation between *in vivo* Aβ retention quantified using PiB PET and postmortem Aβ types including NPs, DPs and CAA in the same neuropathologic ROI, we selected the cases (N = 49) whose neuropathologic assessments were performed at UCSF-NDBB. At UCSF-NDBB, amyloid NP burden was quantified using a modified CERAD score, unadjusted for age according to the UCSF NDBB regional sampling scheme (Mirra et al., 1991). CERAD scores of "absent" or "sparse" were categorized pathologically to be negative, while "moderate" and "frequent" CERAD scores were considered to be positive. DPs were also classified using the same method (Supplementary Fig. 1). CAA severity of "absent" or "positivity in leptomeningeal vessels only" was categorized pathologically to be negative, while "positivity in cortical and/or subcortical vessels" was considered to be positive. Pathologic grading of amyloid was performed prospectively by one of two experienced raters (WWS and LTG) who in some cases had access to the clinical histories and thus may not have been blinded to PiB-PET results.

Template space PiB SUVR were analyzed in five cortical ROI: anterior cingulate cortex, middle frontal gyrus, inferior temporal gyrus, angular gyrus and calcarine cortex (Fig. 2). Custom ROI were created on a template MRI by creating squares centered at coordinates simulating the post-mortem sampling regions in coronal slices, then extending the ROI 3 mm anteriorly and 4mm posteriorly to create an 8 mm thick slice. A total of seven cases were not included in this analysis because of difficulty with PiB data quantification: missing MRI data needed to generate quantitative values for PiB retention (N = 3), inadequate PiB acquisition (N = 3) and failure in realignment due to subject motion (N = 1). Thus, the final sample for analysis included 42 individuals with both quantitative PiB-PET data and Aβ assessment at autopsy (Fig. 1).

2.7. Partial Volume Correction

The primary models were repeated after correcting PiB PET data for partial volume effects. The three-compartment partial volume correction (PVC) method estimates the "true" gray matter signal by adjusting for signal from subjacent white matter and CSF (Muller-Gartner et al., 1992). Gray matter, white matter and CSF probabilities used for PVC were derived from SPM MRI segmentation.

2.8. Statistical analyses

In experiment 1, to determine whether global or regional PiB SUVR would better predict global pathological Aβ burden, receiver-operating characteristic (ROC) analyses were performed. We also explored area under the ROC curve (AUC), and the optimal cut-offs that optimize sensitivity and specificity. DeLong analyses (DeLong et al., 1988) were performed to compare ROC curves between global and regional PiB SUVR.

In experiment 2, to investigate the relationship between *in vivo* imaging and pathological Aβ types in five customized PiB ROIs that correspond to the post-mortem sampling regions, multiple linear regression analyses with the "Enter" method were performed using two models. In Model 1, we entered the period of PET to autopsy and each pathological Aβ type (NPs, DPs, or CAA) as the independent variables and PiB SUVR from the customized ROI as dependent variable. In Model 2, we additionally entered all the resulting statistically significant pathological amyloid aggregates from Model 1 (defined as $p < 0.05$) as independent variables.

Statistical analyses were performed using the Statistical Package for the Social Sciences 18.0 (SPSS Inc.,Chicago,IL) and MedCalc for Windows, version 9.3 (MedCalc Software, Ostend, Belgium).

3. Results

3.1. Experiment 1: global versus regional PiB SUVR

3.1.1. Demographics of participants

Participant characteristics are shown in Table 1. The mean interval between PET scanning and death was 3.1 years (range: 0.2–8.3 years). At the time of PET, 46 subjects had a dementia diagnosis (primarily FTD or AD), six had MCI and two had normal cognition. At autopsy, the most common neuropathological diagnoses were frontotemporal lobar degeneration (FTLD) and AD (often with mixed pathology) (Table 1). The prevalence of amyloid pathologic stages was: 61.1% A0/A1, 38.9% A2/A3 for Thal amyloid phase, and 51.9% C0/C1, 48.1% C2/C3 for CERAD scores. The frequencies of not, low, intermediate and high levels of ADNC were 19.6%, 47.8%, 10.9% and 21.7%, respectively (Table1).

3.1.2. ROC analyses of regional versus global PiB index

The results of the ROC analyses are shown in Table 2. For Thal amyloid phase A2/A3, CERAD NP score C2/C3, and ADNC level intermediate to high, SUVR in the right lateral parietal, left lateral frontal and left lateral frontal regions achieved the highest AUCs (0.917, 0.891, and 0.891), respectively. However, there were no statistical differences between global and highest regional PiB SUVR for Thal phase ($p = 0.186$), CERAD score ($p = 0.230$) and ADNC ($p = 0.221$).

3.1.3. Relationship between global PiB SUVR and ADNC levels

ROC analyses showed that the discrimination of absent from low or higher ADNC was fair (AUC = 0.730), of absent-low from intermediate to high was good (AUC = 0.854), and of absent-moderate from high was excellent (AUC = 0.974) (Supplementary Fig. 2).

3.2. Experiment 2: pathological Aβ types and PiB SUVR

3.2.1. Demographics of participants

The mean interval between PET scanning and death in this subset was 3.3 years (range: 0.2–8.3 years). The overall prevalence of amyloid

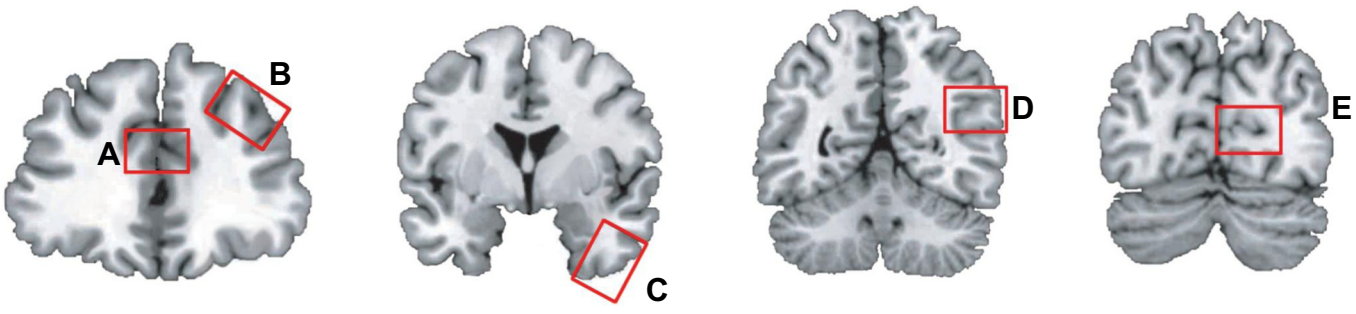

Fig. 2. Five cortical region of interests which Pittsburgh Compound-B standardized uptake value ratio and post-mortem amyloid β burden was analyzed in: (A) anterior cingulate, (B) middle frontal, (C) inferior temporal, (D) angular and (E) calcarine.

Table 2
Receiver operating characteristic results for the detection of Amyloid Thal phase, CERAD score for NP, and ADNC levels.

Amyloid Thal phase, A0 to 1 vs. A2 to 3 (N = 37)	AUC	CERAD score for NPs, C0 to 1 vs. C2 to 3 (N = 54)	AUC	ADNC levels, not-low vs. intermediate-high (N = 54)	AUC
R_lat_parietal	0.917	L_lat_frontal	0.891	L_lat_frontal	0.891
L_lat_parietal	0.910	R_lat_frontal	0.875	R_lat_frontal	0.866
L_precuneus	0.910	L_lat_parietal	0.863	Global	0.854
R_precuneus	0.910	Global	0.854	L_lat_parietal	0.851
R_lat_frontal	0.901	L_med_frontal	0.852	L_precuneus	0.847
L_lat_temporal	0.897	L_precuneus	0.848	L_lat_temporal	0.844
L_occipital	0.894	L_lat_temporal	0.841	L_med_temporal_cortex	0.843
L_lat_frontal	0.891	R_lat_parietal	0.841	R_lat_temporal	0.840
Global	0.888	R_med_frontal	0.841	L_temporal_pole	0.838
L_med_temporal_cortex	0.881	L_med_temporal_cortex	0.837	L_med_frontal	0.835
L_post_cingulate	0.878	R_precuneus	0.837	R_lat_parietal	0.825
L_temporal_pole	0.878	L_striatum	0.832	R_med_frontal	0.824
R_lat_temporal	0.872	R_occipital	0.826	R_temporal_pole	0.816
R_occipital	0.872	L_temporal_pole	0.819	R_med_temporal_cortex	0.813
R_post_cingulate	0.865	L_occipital	0.817	L_striatum	0.810
R_med_frontal	0.865	R_lat_temporal	0.813	R_occipital	0.807
R_temporal_pole	0.853	R_temporal_pole	0.806	L_occipital	0.806
R_med_temporal_cortex	0.849	R_striatum	0.802	R_precuneus	0.796
L_med_frontal	0.849	L_post_cingulate	0.801	L_post_cingulate	0.766
L_striatum	0.843	R_med_temporal_cortex	0.795	R_striatum	0.759
R_striatum	0.837	R_post_cingulate	0.769	R_post_cingulate	0.718
R_hippocampus	0.622	L_hippocampus	0.633	R_hippocampus	0.629
L_hippocampus	0.609	R_hippocampus	0.630	L_hippocampus	0.584

AUC = area under the ROC curve; CERAD = Consortium to Establish a Registry for Alzheimer's Disease; NPs = neuritic plaques; ADNC = Alzheimer's disease neuropathological changes; R = right; L = left; lat = lateral; med = medial; post = posterior.

pathologies was: 59.5% none-sparse/40.5% moderate-frequent for NPs, 52.8%/47.2% for DPs and 82.2% negative/17.8% positive for CAA (Table 1).

3.2.2. Correlation between pathological Aβ types and PiB SUVR

When examined separately (adjusting for PET-autopsy interval) in Model 1, moderate to severe NPs (β = 0.445–0.923, $p < 0.05$) and DPs (β = 0.334–0.844, $p < 0.05$) each correlated with PiB SUVR in all regions (Table 3). CAA also predicted high PiB SUVR in all examined regions (β = 0.410–0.740, $p < 0.05$) (Table 3).

When all the statistically significant pathological Aβ types were included in the same model (Model 2), moderate to severe NPs were independently correlated with PiB SUVR in all regions except for the inferior temporal and calcarine ROI (β = 0.414–0.804, $p < 0.05$), whereas DPs were independently correlated with PiB SUVR in the angular gyrus ROI (β = 0.446, $p = 0.010$), and at a trend level in anterior cingulate ($p = 0.098$) (Table 3). CAA was also associated with PiB SUVR in the inferior temporal and calcarine ROI (β = 0.222–0.355, $p < 0.05$) (Table 3).

Tests for trends across dose dependent amyloid burden (none, sparse, moderate and frequent) showed similar results to those obtained with dichotomous categorization of amyloid aggregates (Supplementary table 1).

We repeated the primary models with partial-volume corrected data. For ROC analyses, results were consistent with those derived from non-PVC data, showing there no differences in the accuracy of detection of amyloid burden or ADNC between regional and global SUVR (Supplementary table 2). We also found that NPs were correlated with PiB SUVR in all ROIs except for the calcarine region, and DPs were correlated with PiB SUVR in the anterior cingulate region (Supplementary table 3).

4. Discussion

We assessed the relationships between *in vivo* imaging and Aβ burden at autopsy. Our major findings were as follows. First, there was no difference in accuracy between regional and global PiB SUVR in predicting pathological Aβ burden as measured by Thal phase or CERAD score. Second, the substrate-specific binding of PiB might differ among the brain specific regions. Taken together, these findings have implications for clinical and research applications of amyloid PET.

Table 3
Association between postmortem types of amyloid β and *in vivo* Pittsburgh Compound-B standardized uptake value ratio in five cortical region of interests.

	Anterior cingulate			Middle frontal			Inferior temporal			Angular			Calcarine		
	B	SE	*p*	B	SE	*p*	B	SE	*p*	B	SE	*p*	B	SE	*p*
Model 1															
Neuritic plaques[a]	0.917	0.135	<0.001	0.923	0.139	<0.001	0.498	0.102	0.001>	0.758	0.139	<0.001	0.445	0.091	<0.001
Diffuse plaques[a]	0.844	0.156	0.001>	0.640	0.175	0.001	0.365	0.116	0.003	0.768	0.139	<0.001	0.334	0.096	0.001
CAA[b]	0.691	0.208	0.002	0.74	0.189	<0.001	0.569	0.106	0.001>	0.652	0.18	0.001	0.41	0.095	<0.001
Model 2															
Neuritic plaques[a]	0.656	0.21	0.003	0.804	0.228	0.001	0.24	0.124	0.062	0.414	0.169	0.019	0.242	0.121	0.053
Diffuse plaques[a]	0.328	0.2	0.11	0.06	0.188	0.752	0.113	0.107	0.297	0.446	0.165	0.01	0.123	0.101	0.23
CAA[b]	0.065	0.194	0.738	0.132	0.206	0.525	0.355	0.131	0.01	0.158	0.174	0.369	0.222	0.106	0.044

Model 1: Multiple linear regressions were performed after controlling for interval from PET to autopsy
Model 2: Postmortem types of Aβ that significantly ($p < 0.05$) correlated with regional PiB retentions were added to Model 1
B (*SE*) = unstandazied β value (standard error of the mean), CAA = cerebral amyloid angiopathy.
[a] Moderate to severe reference to absent to sparse.
[b] "Positivity in cortical and/or subcortical vessels" reference to "absent" or "positivity in leptomeningeal vessels".

4.1. Global versus Regional PiB SUVR for prediction of pathological Aβ burdens

Our first major finding demonstrated that there was no difference in accuracy between peak regional and global PiB SUVR in predicting pathological Aβ burden. While neuropathological staging studies have described amyloid deposition as widely distributed within the association neocortex even at the earliest Thal phase, imaging studies with PiB and other Aβ tracers have highlighted medial prefrontal cortex and precuneus as regions of early tracer retention, particularly in the preclinical state (Mintun et al., 2006; Mormino et al., 2012; Sojkova et al., 2011; Villeneuve et al., 2015). Another study found that patients with intermediate global PiB retention levels (falling below the global threshold for positivity) showed regionally elevated uptake in a variety of regions including dorsolateral prefrontal, medial orbital and temporoparietal cortices (Mormino et al., 2012). Therefore, there may be variability across subjects in the regions showing early PET signal. We found that PiB SUVR in these regions showed numerically higher AUC than global PiB SUVR, but there were no statistical differences in diagnostic accuracy between global and peak regional PiB SUVR. Regional heterogeneity in early PET signal across subjects, or high intercorrelation across regions even at an early stage, may explain why global measures perform as well as regional ones. An important caveat to interpreting these results is that neuropathologic studies are subject to sampling error, and in particular precuneus, an important early region of PiB-PET retention, is not routinely sampled in diagnostic autopsy protocols (including our own), though we did sample anterior cingulate cortex, another important region for early PiB signal (Mintun et al., 2006; Mormino et al., 2012; Sojkova et al., 2011; Villeneuve et al., 2015). It may therefore be that Thal and CERAD scores derived from traditional brain sampling may underestimate early amyloid deposition, and that broader sampling of the brain would show an advantage for regional versus global PiB values. Notably, while the vast majority of our subjects were cognitively impaired, the underlying neuropathological substrates were quite diverse, and our sample did include a broad range of amyloid neuropathology, including sparse and intermediate cases that are critical for assessing early detection. Nevertheless, we recognize that our cohort consisted primarily of patients with clinical dementia at the time of imaging. Our findings need to be reproduced in cohorts consisting primarily of individuals with preclinical or prodromal AD and short PET-to-autopsy intervals in order to assess for generalizability to these populations.

4.2. Global PiB SUVR for prediction of ADNC

We found that even though ADNC includes measures of both amyloid and tau neurofibrillary pathology, global PiB SUVR differentiated ADNC levels. Considering that Braak neurofibrillary score is correlated with amyloid Aβ burden (Murray et al., 2015), it might be reasonable to expect that PiB SUVR would differentiate ADNC levels as well. Although the accuracies of the PiB SUVR for intermediate to high or high levels of ADNC were “good” or “excellent”, the accuracy for low levels of ADNC, as seen in the earliest preclinical stage of AD, was just “fair”. While it is conceivable that other neurodegenerative protein aggregates found post-mortem may have impacted our study, this is unlikely since post-mortem binding and correlative studies have demonstrated high selectivity for PIB to bind to Abeta versus tau or synuclein aggregates (Bacskai et al., 2007; Ikonomovic et al., 2008; Kantarci et al., 2012; Klunk et al., 2003). Previous studies have shown that PIB uptake in clinically diagnosed (Engler et al., 2008; Rabinovici et al., 2011; Rowe et al., 2007) and autopsy confirmed (Villeneuve et al., 2015) patients with FTLD-Tau or FTLD-TDP does not differ from binding in amyloid-negative normal controls. Similarly studies applying other beta-amyloid tracers did not find that mixed pathologies modified amyloid PET signal (Dugger et al., 2014).

4.3. Regional correlations between in vivo amyloid imaging and post-mortem burden of amyloid species

Our second major finding that the substrate-specific binding of PiB might differ among the brain specific regions is supported by the following observations: (1) moderate to severe NPs were independently correlated with PiB SUVR in all regions except for the inferior temporal and calcarine ROI; (2) CAA was associated with PiB SUVR in the inferior temporal and calcarine ROI. Overall, our findings are consistent with the notion that PiB binding is proportional to the fibrillar content of the Aβ lesion (Klunk et al., 2003). Previous studies applying PiB as well as fluorine-18 labelled Aβ tracers, showed that high cortical retention reliably discriminates CERAD moderate-frequent NPs density from absent-low NPs (Clark et al., 2012; Curtis et al., 2015; Murray et al., 2015; Sabri et al., 2015). On the other hand, other studies found that clinical probable CAA patients had occipital predominant PiB uptake, reflecting the predilection of CAA for occipital areas (Bacskai et al., 2007; Ly et al., 2010). In the present study, significant relationships between CAA and PiB SUVR were observed in the inferior temporal as well as calcarine ROI, consistent with the early involvement of inferior temporal cortex in CAA (Thal et al., 2003). Interestingly, we found that DPs contribute to PiB uptake in the angular gyrus after adjusting for NPs. A previous study applying autoradiography to post-mortem samples showed that PiB delineates DPs and CAA as well as NPs (Lockhart et al., 2007). Furthermore, single case reports have highlighted high PiB retention that can be indistinguishable from an AD pattern in patients with very high density DPs and low NPs (Kantarci et al., 2012). Discrepancies between previous studies and our findings may be due to differences in study populations. In general, our sample showed high regional overlap between NPs, DPs and CAA. We did not have a significant number of patients with DLB, who tend to show disproportionate DPs relative to NPs. Therefore, while the majority of PiB signal seems to emanate from highly fibrillar NPs, a high density of DPs (despite lower fibrillarity) or CAA can lead to similar levels of tracer retention.

4.4. Strengths and limitations

Strengths of our study include the prospective setting, and the standardized pathology and PiB-PET imaging protocol. Furthermore, pathological amyloid-beta aggregates and *in vivo* amyloid imaging were measured in comparable ROIs, which enabled us to investigate direct pathological and in vivo imaging correlates of amyloid aggregate types. Some methodological issues need to be considered. First, there was an average 3.3 years interval from amyloid imaging to autopsy. Although we controlled for this interval in the analyses, the prolonged delay in some cases leaves open the possibility that significant Aβ pathology evolved after PiB-PET and prior to death. This argument is mitigated to some degree by the very slow observed annual rates of change in PiB signal in longitudinal studies (Kemppainen et al., 2014; Ossenkoppele et al., 2012). Next, our assessment of pathological Aβ was semi-quantitative, and does not allow true correlation of pathological Aβ as a continuous measure (Ikonomovic et al., 2008). Third, amyloid burden was only assessed in a subset of brain regions. In addition to potential sampling error in the cortex, we did not investigate the role of DPs in subcortical structures where DPs are known to be predominant (Suenaga et al., 1990), or of amyloid species in the cerebellum which was used as the reference region for SUVR (Suenaga et al., 1990). Fourth, our sample size might render us under-powered to detect partial correlations of DPs or CAA after adjusting for NPs. This possibility is supported by a number of trend-level results in the combined model. Finally, an important methodological consideration is that diffuse and neuritic amyloid plaque densities are estimated at our center based on morphological features seen on abeta IHC. Results may therefore differ from those obtained with amyloid-tau double immunostaining or silver staining. Generalizability of our findings may be limited by the unique composition of our sample, which, by virtue of the clinical

studies through which patients were imaged, was enriched for patients with FTLD and AD neuropathology.

4.5. Conclusions

In conclusion, there was no difference in accuracy between regional and global PiB SUVR in predicting pathological Aβ burden. We also found that regional PiB signal was dominated by NPs. Therefore, our findings advance our understanding of the correlations between amyloid PET and neuropathological Aβ, and have implications for the future use of Aβ PET in clinical practice, observational research and drug development.

Author contributions

Drs. Sang Won Seo had full access to all of the data in the study and take responsibility for the integrity of the data and the accuracy of the data analysis.

Study concept and design: Sang Won Seo, Nagehan Ayakta, Gil D. Rabinovici

Acquisition, analysis, or interpretation of data: Sang Won Seo, Nagehan Ayakta, Lea T. Grinberg, Sylvia Villeneuve, Manja Lehmann, Bruce Reed, Charles DeCarli, Bruce L. Miller, Howard J. Rosen, Adam L. Boxer, William J. Jagust, James P. O'Neil, Lee-Way Jin, William W. Seeley, Gil D. Rabinovici.

Critical revision of the manuscript for important intellectual content: Sang Won Seo, Nagehan Ayakta, Lea T. Grinberg, Sylvia Villeneuve, Manja Lehmann, Bruce Reed, Charles DeCarli, Bruce L. Miller, Howard J. Rosen, Adam L. Boxer, William J. Jagust, James P. O'Neil, Lee-Way Jin, William W. Seeley, Gil D. Rabinovici.

Drafting of the manuscript: Sang Won Seo, Nagehan Ayakta, Gil D. Rabinovici.

Study funding

This work was supported National Institute on Aging grants K23-AG031861 and R01-AG045611 to G.D.R., P01-AG1972403 to B.LM. and W.W.S, P50-AG023501 to B.L.M., G.D.R and W.W.S., P01-AG12435, P30-AG10129, R01-AG021028 and R01-AG031563 to C.D., R01-AG031563 to B.R.; R01-AG034570 to WJJ; the Consortium for Frontotemporal Dementia Research to B.L.M. and W.W.S; the Tau Consortium to W.W.S., G.D.R and W.J.J.; John Douglas French Alzheimer's Foundation to G.D.R. and B.L.M.; State of California Department of Health Services Alzheimer's Disease Research Center of California grant 04-33516 to B.L.M.; the National Research Foundation of Korea grants (2016M3C7A1913844) to S.W.S.

Disclosure

Dr. Rabinovici received consulting or speaking honoraria from Eisai, GE Healthcare, Medscape, Piramal Imaging, Putnam and Lundbeck, and receives research support from Avid Radiopharmaceuticals, GE Healthcare and Piramal Imaging. Dr. Grinberg receives research support from Avid Radiopharmaceuticals.

Dr. Jagust serves as a consultant to Bioclinica, Banner Alzheimer Institute, Genentech, and Novartis.

Acknowledgments

We would like to acknowledge Suzanne Baker, Mustafa Janabi, Kris Norton for their support with PET scanning; and Dennis Dickson, Mario Mendez, John Trojanowski and Harry Vinters for patient referrals and autopsies.

Appendix A. Supplementary data

Supplementary data to this article can be found online at http://dx.doi.org/10.1016/j.nicl.2016.11.008.

References

Albert, M.S., DeKosky, S.T., Dickson, D., Dubois, B., Feldman, H.H., Fox, N.C., Gamst, A., Holtzman, D.M., Jagust, W.J., Petersen, R.C., Snyder, P.J., Carrillo, M.C., Thies, B., Phelps, C.H., 2011. The diagnosis of mild cognitive impairment due to Alzheimer's disease: recommendations from the National Institute on Aging-Alzheimer's Association workgroups on diagnostic guidelines for Alzheimer's disease. Alzheimers Dement. 7, 270–279.

Armstrong, M.J., Litvan, I., Lang, A.E., Bak, T.H., Bhatia, K.P., Borroni, B., Boxer, A.L., Dickson, D.W., Grossman, M., Hallett, M., Josephs, K.A., Kertesz, A., Lee, S.E., Miller, B.L., Reich, S.G., Riley, D.E., Tolosa, E., Troster, A.I., Vidailhet, M., Weiner, W.J., 2013. Criteria for the diagnosis of corticobasal degeneration. Neurology 80, 496–503.

Bacskai, B.J., Frosch, M.P., Freeman, S.H., Raymond, S.B., Augustinack, J.C., Johnson, K.A., Irizarry, M.C., Klunk, W.E., Mathis, C.A., Dekosky, S.T., Greenberg, S.M., Hyman, B.T., Growdon, J.H., 2007. Molecular imaging with Pittsburgh Compound B confirmed at autopsy: a case report. Arch. Neurol. 64, 431–434.

Clark, C.M., Pontecorvo, M.J., Beach, T.G., Bedell, B.J., Coleman, R.E., Doraiswamy, P.M., Fleisher, A.S., Reiman, E.M., Sabbagh, M.N., Sadowsky, C.H., Schneider, J.A., Arora, A., Carpenter, A.P., Flitter, M.L., Joshi, A.D., Krautkramer, M.J., Lu, M., Mintun, M.A., Skovronsky, D.M., 2012. Cerebral PET with florbetapir compared with neuropathology at autopsy for detection of neuritic amyloid-beta plaques: a prospective cohort study. Lancet Neurol. 11, 669–678.

Curtis, C., Gamez, J.E., Singh, U., Sadowsky, C.H., Villena, T., Sabbagh, M.N., Beach, T.G., Duara, R., Fleisher, A.S., Frey, K.A., Walker, Z., Hunjan, A., Holmes, C., Escovar, Y.M., Vera, C.X., Agronin, M.E., Ross, J., Bozoki, A., Akinola, M., Shi, J., Vandenberghe, R., Ikonomovic, M.D., Sherwin, P.F., Grachev, I.D., Farrar, G., Smith, A.P., Buckley, C.J., McLain, R., Salloway, S., 2015. Phase 3 trial of flutemetamol labeled with radioactive fluorine 18 imaging and neuritic plaque density. JAMA Neurol. 72, 287–294.

DeLong, E.R., DeLong, D.M., Clarke-Pearson, D.L., 1988. Comparing the areas under two or more correlated receiver operating characteristic curves: a nonparametric approach. Biometrics 44, 837–845.

Dickson, D.W., Farlo, J., Davies, P., Crystal, H., Fuld, P., Yen, S.H., 1988. Alzheimer's disease. A double-labeling immunohistochemical study of senile plaques. Am. J. Pathol. 132, 86–101.

Dugger, B.N., Clark, C.M., Serrano, G., Mariner, M., Bedell, B.J., Coleman, R.E., Doraiswamy, P.M., Lu, M., Fleisher, A.S., Reiman, E.M., Sabbagh, M.N., Sadowsky, C.H., Schneider, J.A., Zehntner, S.P., Carpenter, A.P., Joshi, A.D., Mintun, M.A., Pontecorvo, M.J., Skovronsky, D.M., Sue, L.I., Beach, T.G., 2014. Neuropathologic heterogeneity does not impair florbetapir-positron emission tomography postmortem correlates. J. Neuropathol. Exp. Neurol. 73, 72–80.

Engler, H., Santillo, A.F., Wang, S.X., Lindau, M., Savitcheva, I., Nordberg, A., Lannfelt, L., Langstrom, B., Kilander, L., 2008. In vivo amyloid imaging with PET in frontotemporal dementia. Eur. J. Nucl. Med. Mol. Imaging 35, 100–106.

Gorno-Tempini, M.L., Hillis, A.E., Weintraub, S., Kertesz, A., Mendez, M., Cappa, S.F., Ogar, J.M., Rohrer, J.D., Black, S., Boeve, B.F., Manes, F., Dronkers, N.F., Vandenberghe, R., Rascovsky, K., Patterson, K., Miller, B.L., Knopman, D.S., Hodges, J.R., Mesulam, M.M., Grossman, M., 2011. Classification of primary progressive aphasia and its variants. Neurology 76, 1006–1014.

Hyman, B.T., Phelps, C.H., Beach, T.G., Bigio, E.H., Cairns, N.J., Carrillo, M.C., Dickson, D.W., Duyckaerts, C., Frosch, M.P., Masliah, E., Mirra, S.S., Nelson, P.T., Schneider, J.A., Thal, D.R., Thies, B., Trojanowski, J.Q., Vinters, H.V., Montine, T.J., 2012. National Institute on Aging-Alzheimer's Association guidelines for the neuropathologic assessment of Alzheimer's disease. Alzheimers Dement. 8, 1–13.

Ikonomovic, M.D., Klunk, W.E., Abrahamson, E.E., Mathis, C.A., Price, J.C., Tsopelas, N.D., Lopresti, B.J., Ziolko, S., Bi, W., Paljug, W.R., Debnath, M.L., Hope, C.E., Isanski, B.A., Hamilton, R.L., DeKosky, S.T., 2008. Post-mortem correlates of in vivo PiB-PET amyloid imaging in a typical case of Alzheimer's disease. Brain 131, 1630–1645.

Kantarci, K., Yang, C., Schneider, J.A., Senjem, M.L., Reyes, D.A., Lowe, V.J., Barnes, L.L., Aggarwal, N.T., Bennett, D.A., Smith, G.E., Petersen, R.C., Jack Jr., C.R., Boeve, B.F., 2012. Antemortem amyloid imaging and beta-amyloid pathology in a case with dementia with Lewy bodies. Neurobiol. Aging 33, 878–885.

Kemppainen, N.M., Scheinin, N.M., Koivunen, J., Johansson, J., Toivonen, J.T., Nagren, K., Rokka, J., Karrasch, M., Parkkola, R., Rinne, J.O., 2014. Five-year follow-up of 11C-PIB uptake in Alzheimer's disease and MCI. Eur. J. Nucl. Med. Mol. Imaging 41, 283–289.

Klunk, W.E., Wang, Y., Huang, G.F., Debnath, M.L., Holt, D.P., Shao, L., Hamilton, R.L., Ikonomovic, M.D., DeKosky, S.T., Mathis, C.A., 2003. The binding of 2-(4′-methylaminophenyl)benzothiazole to postmortem brain homogenates is dominated by the amyloid component. J. Neurosci. 23, 2086–2092.

Lockhart, A., Lamb, J.R., Osredkar, T., Sue, L.I., Joyce, J.N., Ye, L., Libri, V., Leppert, D., Beach, T.G., 2007. PIB is a non-specific imaging marker of amyloid-beta (Abeta) peptide-related cerebral amyloidosis. Brain 130, 2607–2615.

Ly, J.V., Donnan, G.A., Villemagne, V.L., Zavala, J.A., Ma, H., O'Keefe, G., Gong, S.J., Gunawan, R.M., Saunder, T., Ackerman, U., Tochon-Danguy, H., Churilov, L., Phan, T.G., Rowe, C.C., 2010. 11C-PIB binding is increased in patients with cerebral amyloid angiopathy-related hemorrhage. Neurology 74, 487–493.

Mackenzie, I.R., Neumann, M., Bigio, E.H., Cairns, N.J., Alafuzoff, I., Kril, J., Kovacs, G.G., Ghetti, B., Halliday, G., Holm, I.E., Ince, P.G., Kamphorst, W., Revesz, T., Rozemuller, A.J., Kumar-Singh, S., Akiyama, H., Baborie, A., Spina, S., Dickson, D.W., Trojanowski, J.Q., Mann, D.M., 2010. Nomenclature and nosology for neuropathologic subtypes of frontotemporal lobar degeneration: an update. Acta Neuropathol. 119, 1–4.

McKhann, G.M., Knopman, D.S., Chertkow, H., Hyman, B.T., Jack Jr., C.R., Kawas, C.H., Klunk, W.E., Koroshetz, W.J., Manly, J.J., Mayeux, R., Mohs, R.C., Morris, J.C., Rossor, M.N., Scheltens, P., Carrillo, M.C., Thies, B., Weintraub, S., Phelps, C.H., 2011. The

diagnosis of dementia due to Alzheimer's disease: recommendations from the National Institute on Aging-Alzheimer's Association workgroups on diagnostic guidelines for Alzheimer's disease. Alzheimers Dement. 7, 263–269.
Mintun, M.A., Larossa, G.N., Sheline, Y.I., Dence, C.S., Lee, S.Y., Mach, R.H., Klunk, W.E., Mathis, C.A., DeKosky, S.T., Morris, J.C., 2006. [11C]PIB in a nondemented population: potential antecedent marker of Alzheimer disease. Neurology 67, 446–452.
Mirra, S.S., Heyman, A., McKeel, D., Sumi, S.M., Crain, B.J., Brownlee, L.M., Vogel, F.S., Hughes, J.P., van Belle, G., Berg, L., 1991. The Consortium to Establish a Registry for Alzheimer's Disease (CERAD). Part II. Standardization of the neuropathologic assessment of Alzheimer's disease. Neurology 41, 479–486.
Montine, T.J., Phelps, C.H., Beach, T.G., Bigio, E.H., Cairns, N.J., Dickson, D.W., Duyckaerts, C., Frosch, M.P., Masliah, E., Mirra, S.S., Nelson, P.T., Schneider, J.A., Thal, D.R., Trojanowski, J.Q., Vinters, H.V., Hyman, B.T., 2012. National Institute on Aging-Alzheimer's Association guidelines for the neuropathologic assessment of Alzheimer's disease: a practical approach. Acta Neuropathol. 123, 1–11.
Mormino, E.C., Brandel, M.G., Madison, C.M., Rabinovici, G.D., Marks, S., Baker, S.L., Jagust, W.J., 2012. Not quite PIB-positive, not quite PIB-negative: slight PIB elevations in elderly normal control subjects are biologically relevant. NeuroImage 59, 1152–1160.
Muller-Gartner, H.W., Links, J.M., Prince, J.L., Bryan, R.N., McVeigh, E., Leal, J.P., Davatzikos, C., Frost, J.J., 1992. Measurement of radiotracer concentration in brain gray matter using positron emission tomography: MRI-based correction for partial volume effects. J. Cereb. Blood Flow Metab. 12, 571–583.
Murray, M.E., Lowe, V.J., Graff-Radford, N.R., Liesinger, A.M., Cannon, A., Przybelski, S.A., Rawal, B., Parisi, J.E., Petersen, R.C., Kantarci, K., Ross, O.A., Duara, R., Knopman, D.S., Jack Jr., C.R., Dickson, D.W., 2015. Clinicopathologic and 11C-Pittsburgh compound B implications of Thal amyloid phase across the Alzheimer's disease spectrum. Brain 138, 1370–1381.
Ogomori, K., Kitamoto, T., Tateishi, J., Sato, Y., Suetsugu, M., Abe, M., 1989. Beta-protein amyloid is widely distributed in the central nervous system of patients with Alzheimer's disease. Am. J. Pathol. 134, 243–251.
Ossenkoppele, R., Tolboom, N., Foster-Dingley, J.C., Adriaanse, S.F., Boellaard, R., Yaqub, M., Windhorst, A.D., Barkhof, F., Lammertsma, A.A., Scheltens, P., van der Flier, W.M., van Berckel, B.N., 2012. Longitudinal imaging of Alzheimer pathology using [11C]PIB, [18F]FDDNP and [18F]FDG PET. Eur. J. Nucl. Med. Mol. Imaging 39, 990–1000.
Petersen, R.C., 2004. Mild cognitive impairment as a diagnostic entity. J. Intern. Med. 256, 183–194.
Rabinovici, G.D., Furst, A.J., Alkalay, A., Racine, C.A., O'Neil, J.P., Janabi, M., Baker, S.L., Agarwal, N., Bonasera, S.J., Mormino, E.C., Weiner, M.W., Gorno-Tempini, M.L., Rosen, H.J., Miller, B.L., Jagust, W.J., 2010. Increased metabolic vulnerability in early-onset Alzheimer's disease is not related to amyloid burden. Brain 133, 512–528.
Rabinovici, G.D., Rosen, H.J., Alkalay, A., Kornak, J., Furst, A.J., Agarwal, N., Mormino, E.C., O'Neil, J.P., Janabi, M., Karydas, A., Growdon, M.E., Jang, J.Y., Huang, E.J., Dearmond, S.J., Trojanowski, J.Q., Grinberg, L.T., Gorno-Tempini, M.L., Seeley, W.W., Miller, B.L., Jagust, W.J., 2011. Amyloid vs FDG-PET in the differential diagnosis of AD and FTLD. Neurology 77, 2034–2042.
Rascovsky, K., Hodges, J.R., Knopman, D., Mendez, M.F., Kramer, J.H., Neuhaus, J., van Swieten, J.C., Seelaar, H., Dopper, E.G., Onyike, C.U., Hillis, A.E., Josephs, K.A., Boeve, B.F., Kertesz, A., Seeley, W.W., Rankin, K.P., Johnson, J.K., Gorno-Tempini, M.L., Rosen, H., Prioleau-Latham, C.E., Lee, A., Kipps, C.M., Lillo, P., Piguet, O., Rohrer, J.D., Rossor, M.N., Warren, J.D., Fox, N.C., Galasko, D., Salmon, D.P., Black, S.E., Mesulam, M., Weintraub, S., Dickerson, B.C., Diehl-Schmid, J., Pasquier, F., Deramecourt, V., Lebert, F., Pijnenburg, Y., Chow, T.W., Manes, F., Grafman, J., Cappa, S.F., Freedman, M., Grossman, M., Miller, B.L., 2011. Sensitivity of revised diagnostic criteria for the behavioural variant of frontotemporal dementia. Brain 134, 2456–2477.
Rowe, C.C., Ng, S., Ackermann, U., Gong, S.J., Pike, K., Savage, G., Cowie, T.F., Dickinson, K.L., Maruff, P., Darby, D., Smith, C., Woodward, M., Merory, J., Tochon-Danguy, H., O'Keefe, G., Klunk, W.E., Mathis, C.A., Price, J.C., Masters, C.L., Villemagne, V.L., 2007. Imaging beta-amyloid burden in aging and dementia. Neurology 68, 1718–1725.
Sabri, O., Sabbagh, M.N., Seibyl, J., Barthel, H., Akatsu, H., Ouchi, Y., Senda, K., Murayama, S., Ishii, K., Takao, M., Beach, T.G., Rowe, C.C., Leverenz, J.B., Ghetti, B., Ironside, J.W., Catafau, A.M., Stephens, A.W., Mueller, A., Koglin, N., Hoffmann, A., Roth, K., Reininger, C., Schulz-Schaeffer, W.J., Florbetaben Phase 3 Study Group, 2015. Florbetaben PET imaging to detect amyloid beta plaques in Alzheimer's disease: phase 3 study. Alzheimers Dement. 11, 964–974.
Sojkova, J., Driscoll, I., Iacono, D., Zhou, Y., Codispoti, K.E., Kraut, M.A., Ferrucci, L., Pletnikova, O., Mathis, C.A., Klunk, W.E., O'Brien, R.J., Wong, D.F., Troncoso, J.C., Resnick, S.M., 2011. In vivo fibrillar beta-amyloid detected using [11C]PiB positron emission tomography and neuropathologic assessment in older adults. Arch. Neurol. 68, 232–240.
Suenaga, T., Hirano, A., Llena, J.F., Yen, S.H., Dickson, D.W., 1990. Modified Bielschowsky stain and immunohistochemical studies on striatal plaques in Alzheimer's disease. Acta Neuropathol. 80, 280–286.
Thal, D.R., Ghebremedhin, E., Orantes, M., Wiestler, O.D., 2003. Vascular pathology in Alzheimer disease: correlation of cerebral amyloid angiopathy and arteriosclerosis/lipohyalinosis with cognitive decline. J. Neuropathol. Exp. Neurol. 62, 1287–1301.
Tzourio-Mazoyer, N., Landeau, B., Papathanassiou, D., Crivello, F., Etard, O., Delcroix, N., Mazoyer, B., Joliot, M., 2002. Automated anatomical labeling of activations in SPM using a macroscopic anatomical parcellation of the MNI MRI single-subject brain. NeuroImage 15, 273–289.
Villeneuve, S., Rabinovici, G.D., Cohn-Sheehy, B.I., Madison, C., Ayakta, N., Ghosh, P.M., La Joie, R., Arthur-Bentil, S.K., Vogel, J.W., Marks, S.M., Lehmann, M., Rosen, H.J., Reed, B., Olichney, J., Boxer, A.L., Miller, B.L., Borys, E., Jin, L.W., Huang, E.J., Grinberg, L.T., DeCarli, C., Seeley, W.W., Jagust, W., 2015. Existing Pittsburgh Compound-B positron emission tomography thresholds are too high: statistical and pathological evaluation. Brain 138, 2020–2033.